

## Simple model of cytoskeletal fluctuations

C. Metzner, C. Raupach, D. Paranhos Zitterbart, and B. Fabry

*Biophysics Group, Department of Physics, University of Erlangen-Nuremberg, Henkestrasse 91, 91052 Erlangen, Germany*

(Received 22 December 2006; revised manuscript received 1 May 2007; published 27 August 2007)

The spontaneous motion of microbeads bound to the cytoskeleton of living cells is not an ordinary random walk. Unlike Brownian motion, the mean-square displacement undergoes a transition from subdiffusive to superdiffusive behavior with time. This transition is associated with characteristic changes of the turning angle distribution. Recent experimental data demonstrated that force fluctuations measured in an elastic hydrogel matrix beneath the cell correlate with the bead motion [C. Raupach *et al.*, Phys. Rev. E **76**, 011918 (2007)]. These data indicate that the bead trajectory is driven by motor forces originating from the actomyosin network and that cytoskeletal remodeling processes with short- and long-time dynamics are mainly responsible for the non-Brownian behavior. We show that the essential statistical properties of the spontaneous bead motion can be reproduced by a particle diffusing in a potential well with a slowly drifting minimum position. Based on this simple model, which can be solved analytically, we develop a biologically plausible numerical model of a tensed and continuously remodeling actomyosin network that accounts quantitatively for the measured data.

DOI: [10.1103/PhysRevE.76.021925](https://doi.org/10.1103/PhysRevE.76.021925)

PACS number(s): 87.16.Ka, 87.16.Ac, 87.15.Ya, 87.15.Vv

### I. INTRODUCTION

Microbead rheology has been used successfully in the past decade as an experimental tool for probing the viscoelastic properties of complex liquids and solids. In passive microrheology, micron-sized beads are dispersed in the material of interest and the spontaneous fluctuations of these markers are tracked [1]. A statistical analysis of the observed random trajectories can then reveal collective properties of the material, in particular the frequency-dependent complex shear modulus.

The bead motion results from an interplay between random molecular forces that drive the bead, and impeding forces from the system's viscoelastic response to the bead motion.<sup>1</sup> When a bead fluctuates spontaneously, a small amount of thermal energy is transferred from the medium to the bead's few macroscopic degrees of freedom. After a short time, the coherent kinetic energy of the bead is again dissipated by the medium. The two processes, representing just different aspects of the same ongoing energy exchange, are therefore linked by fluctuation-dissipation theorems [2].

In the case of inert, nonliving matter, random forces acting on the bead are of thermal origin. Assuming thermal equilibrium, they can usually be considered as white noise with a power spectral density set by the temperature. The statistics of the bead trajectories is then only determined by the response function of the surrounding material, and in practice one can compute a frequency-dependent complex shear modulus from the measured time-dependent mean-square displacement (MSD) [3].

When microrheology is applied to cells, the situation is more complicated. Living cells are highly dynamic, adaptive systems in a state far from equilibrium. Adenosine triphosphate (ATP)-driven motor proteins are able to create nonthermal, localized, temporally correlated, and spatially directed

forces. In addition, several motors can cooperate in an organized way to create collectively strong, persisting traction. This happens, for example, in stress fibers, resembling a kind of "micromuscle" within a cell. It is not obvious how to separate "random" force fluctuations, occurring on various time scales, from a coordinated activity in such systems.

The pronounced inhomogeneity of the cytosol and the cytoskeleton raises further conceptual problems. Nevertheless, in active microrheological experiments, cells can be treated as an effective (averaged) medium with well-defined viscoelastic material properties. Several groups, using different experimental methods, have found a universal, weak power-law behavior for the complex elastic modulus [4–8]. In this respect, living cells resemble inert materials with so-called soft glassy rheology. A general mechanism able to explain this power-law rheology has been presented by Sollich *et al.* [9].

In the spirit of the effective medium approach, the known response function of the cell can be combined with the MSD data from spontaneous bead (or endogeneous marker) fluctuations, in order to deduce the properties of the driving forces. This idea was proposed by Lau *et al.* [10], who demonstrated that the force fluctuations are much stronger than thermal noise. They further concluded from their data that the power spectrum should follow a  $\omega^{-2}$  law. However, the interpretation of the power spectrum in terms of point motors dispersed throughout the intracellular medium has recently been challenged [11].

In this report, we refer to recent experiments [12] in which we observed the spontaneous motion of beads coated with fibronectin. Cells recognize the coating as a "substrate" and form focal adhesions (FAs) at the bead surfaces, thus tightly connecting them to the cytoskeleton. The beads then started to move in a random, yet clearly non-Brownian way, which was analyzed statistically in detail. Superimposed onto a rapid random diffusion, the bead trajectories often showed periods of slow drift along some persistent directions, separated by major turns (see Fig. 1).

At the same time, markers embedded in an elastic polyacrylamide substrate beneath the cell fluctuated in close cor-

<sup>1</sup>In active microrheology, the viscoelastic response function can be measured independently by applying controlled external forces on the bead.

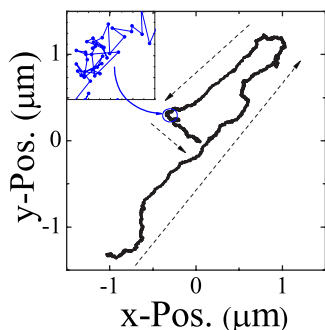


FIG. 1. (Color online) An example of a measured bead trajectory, demonstrating phases of persistent motion (marked by dashed arrows), separated by occasional major turns. The inset shows an enlarged detail (box width of 40 nm).

relation with the intracellular beads. This suggests strongly that the main driving forces of the observed motions originate from the cytoskeletal network, which is mechanically coupled, via transmembrane receptors, to both the beads and the extracellular substrate. Hence, a motor-driven network model, rather than an effective medium approach with point motors, seems more appropriate for describing the system.

Using only *in vitro* actin networks with passive crosslinkers, Gardel *et al.* [13,14] could qualitatively reproduce the mechanical power-law response of cells. When prestressed, these passive networks showed a nonlinear stress stiffening similar to real cells. The existence of such prestress in actomyosin stress fibers has, for example, been clearly demonstrated by Kumar *et al.* [15]. The mechanical properties of single stress fibers have been investigated by Deguchi *et al.* [16].

Taken together, the cytoskeletal network is a highly complex system of different polymer filaments and filaments bundled into fibers, as well as various types of cross-linkers and motor proteins. In order to develop useful approximations of this complex situation it is thus crucial to identify (and restrict oneself to) the most relevant key components. As we will demonstrate below, prominent experimental observations can be reproduced by a network of actomyosin stress fibers as a minimum system.

## II. EXPERIMENTS

For our experiments, MeWo skin carcinoma cells were plated onto 35-mm culture dishes (Nunc surface) and grown to confluence overnight in an incubator (5% CO<sub>2</sub>, 37 °C). Carboxylated fluorescent polystyrene beads (Molecular Probes, Eugene, OR) with a radius of 2 μm were coated with fibronectin (Roche Applied Science) and bound to the cells via integrin receptors 30 min prior to measurements. Fluorescent images were recorded with a charge-coupled-device camera (Hamamatsu Orca-ER) mounted on an inverted microscope with a 10× (0.3 NA) objective. Bead positions of typically 50–200 beads per field of view were tracked continuously for 5 min by computing the intensity-weighted average (center of mass) of each bead [accuracy 10 nm (rms) for 10× magnification of the objective] and

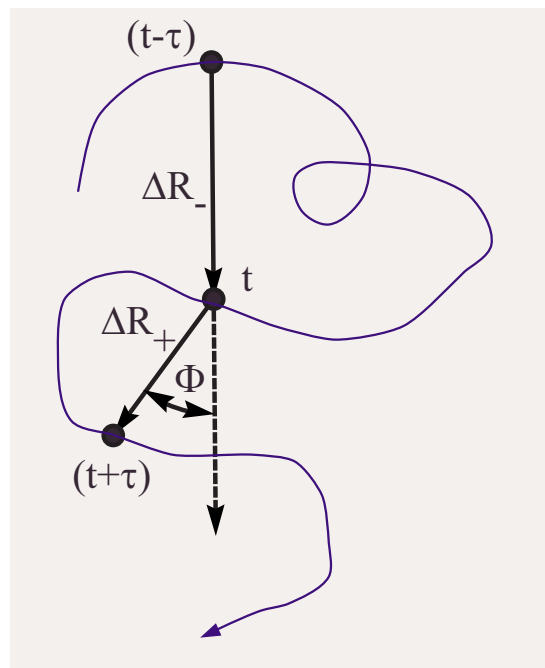


FIG. 2. (Color online) Schematic trajectory, demonstrating the definition of the shift vectors and the turning angle.

corrected for the effects of microscope stage drift. Details of the measurement procedure can be found in [12].

## III. QUANTIFYING TRAJECTORIES

The raw data provided by bead tracking experiments are two-dimensional particle trajectories  $\vec{R}(t)$ , recorded with a fixed sample rate  $1/\delta t$  up to a maximum observation time  $T_{obs}$ . The trajectories vary greatly—even in their qualitative aspects—from one measurement to the next.<sup>2</sup> It is therefore essential to define suitable statistical averages in order to extract meaningful and generalizable information from an ensemble of trajectories. In this section we introduce the main statistical quantities that will be used in this work.

Figure 2 shows three marked points along a particle trajectory, taken at the times  $(t-\tau)$ ,  $t$  and  $(t+\tau)$ . Here and in the following,  $t$  is called the “absolute time” and  $\tau$  the “lag time.” The vectors

$$\Delta\vec{R}_- = \vec{R}(t) - \vec{R}(t - \tau),$$

$$\Delta\vec{R}_+ = \vec{R}(t + \tau) - \vec{R}(t) \quad (1)$$

describe the displacements of the particle between the successive marked points. The MSD is defined as

<sup>2</sup>Even within a confluent monolayer of cells the statistical properties of beads are strongly inhomogeneous with respect to space and time. One of the important factors here may be the different degree of internalization of the beads into the cell and how strongly they bind to the cytoskeleton.

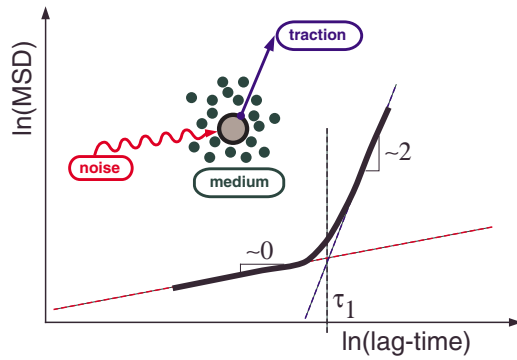


FIG. 3. (Color online) Schematic illustration of the experimentally observed transition from subdiffusive to superdiffusive behavior. It is interpreted as a cross-over between two power-law regimes. The inset shows the physical components that are relevant for this feature.

$$\Delta R^2(\tau) = \left\langle \frac{1}{2} [|\Delta \vec{R}_-|^2 + |\Delta \vec{R}_+|^2] \right\rangle_t, \quad (2)$$

where  $\langle \dots \rangle_t$  stands for an average over the absolute time  $t$ .

A useful dimensionless parameter is the local slope of the “MSD-versus-lag time” curve in a double-logarithmic plot:

$$b(\tau) = \frac{d \ln[\overline{\Delta R^2}(\tau)/\lambda^2]}{d \ln[\tau/\delta t]}, \quad (3)$$

where  $\lambda = \sqrt{\overline{\Delta R^2}(\tau = \delta t)}$  is the average bead displacement during one sampling interval  $\delta t$ . Here  $b$  can be interpreted as an instantaneous or “local” power-law exponent: For standard random walks,  $b=1$ ; for subdiffusive  $b < 1$  and superdiffusive processes,  $b > 1$  [17].

Another important quantity is the so-called turning angle  $\Phi \in [-\pi, \dots, +\pi]$ , defined as the angle enclosed between two successive shift vectors  $\Delta \vec{R}_-$  and  $\Delta \vec{R}_+$  (Fig. 2):

$$\Phi(\tau, t) = \angle(\Delta \vec{R}_-, \Delta \vec{R}_+). \quad (4)$$

The turning angle distribution (TAD) can be expressed as

$$P(\Phi, \tau) = \langle \delta(\Phi - \Phi(\tau, t)) \rangle_t. \quad (5)$$

#### IV. ESSENTIAL SYSTEM COMPONENTS

A main finding of our experimental work was a transition in the MSD from subdiffusive to superdiffusive behavior at lag times around  $\tau_1 = 1$  s. As drawn schematically in Fig. 3, this suggests a crossover from a flat to a steep power law. The inset of the figure also shows the major physical factors which play a role in determining the observed bead motion.

The medium is defined here as the combined system of cytoskeleton and cytosol. In an average sense, it can be described by a rheological response function, relating a given applied force profile to the resulting temporal displacement. The shear modulus  $G(s)$  of living cells as a function of Laplace frequency  $s = i\omega$  has been measured by active microrheology with cytoskeleton-bound beads [5] and was

found to follow a weak power law  $G(s) \propto s^\beta$  superimposed onto a linear background viscosity term  $s\eta$ . The small exponent  $\beta \approx 0.2$  means that the response is predominantly elastic.

The noise term that drives the bead motion includes all rapidly and randomly fluctuating forces acting on the bead. Besides thermal fluctuations, which can be described by temperature-dependent white noise, we have to consider noise created by motor protein activity. The power spectrum of the noise generated by ATP-powered motor proteins will in general be frequency dependent. However, in the limit of very small frequencies (below some rollover frequency in the millisecond range) the spectrum becomes flat. Since we are interested here in the temporal regime around 1 s, the motor noise, too, can be modeled as being effectively white (see Fig. 9).

Taken together, we argue that the flat, subdiffusive power law in Fig. 3 can be attributed to a diffusion of the bead in the complex medium described by  $G(s)$  and  $s\eta$ , driven by white noise of thermal as well as active origin.

The driving force responsible for the steep power law, which signifies almost ballistic bead motion (constant drift velocity, MSD exponent  $\approx 2$ ), must exhibit a certain degree of persistence. If the medium were purely viscous, a constant traction force ( $\propto t^0$ ) could account for the ballistic motion. An elastic medium requires a traction force that grows linearly with time ( $\propto t^1$ ) for a substantial period—in other words, a force ramp. In reality, the shear modulus of the cellular medium has a small fractional power-law exponent, so that the lower bound for the temporal exponent of the traction force is somewhat smaller than 1.

In the following, we will approximate the system as a particle in two dimensions, bound elastically in a well and simultaneously submerged in a viscous background liquid. The particle is driven by white noise forces, as well as persistent force ramps. This situation can be captured in the simple picture of “diffusion in a drifting potential well.”

#### V. DRIFTING WELL MODEL

##### A. Diffusion in a potential well

We consider the two-dimensional spontaneous motion of a test particle, suspended in a fluid and simultaneously bound in a harmonic potential well. Neglecting inertia effects (overdamped Langevin dynamics), we decompose the forces acting on the particle as follows:

$$\vec{F}^{(tot)} = \vec{F}^{(rnd)} + \vec{F}^{(fri)} + \vec{F}^{(ela)}. \quad (6)$$

The noise term  $\vec{F}^{(rnd)}$  represents the driving forces due to the molecular agitation of the background fluid. In the following we will use white noise with a power density of  $\Gamma_w$  and statistically independent spatial components. The damping term is modeled by a linear friction force, proportional to the momentary velocity  $\vec{v}(t)$  of the particle:

$$\vec{F}^{(fri)}(t) = -\alpha \vec{v}(t). \quad (7)$$

The binding of the particle is described by an isotropic elastic potential well of stiffness  $k_w$ , centered at the origin  $\vec{R}_{ctr}$

$=\vec{0}$ . This corresponds to a potential energy function  $U = (k_w/2)R^2$  and produces a binding force  $F^{(ela)}(\vec{R}) = -k_w\vec{R}$ , so that

$$\vec{F}^{(tot)} = \vec{F}^{(md)} + \vec{F}^{(fri)} + \vec{F}^{(ela)}. \quad (8)$$

The global MSD of this system can be computed analytically (for the derivation see the Appendix):

$$\overline{\Delta R^2}(\tau) = \frac{2\Gamma_w}{k_w\alpha}(1 - e^{-(k_w/\alpha)\tau}). \quad (9)$$

It is useful here to define a characteristic relaxation time

$$\tau_0 = \alpha/k_w. \quad (10)$$

For small lag times  $\tau \ll \tau_0$ , the exponential function can be expanded to first order in  $\tau$ , yielding

$$\overline{\Delta R^2}(\tau \rightarrow 0) = 2(\Gamma_w/\alpha^2)\tau. \quad (11)$$

In this regime, the binding force plays no role and the particle diffuses freely with the diffusion constant<sup>3</sup>

$$D = \Gamma_w/(2\alpha^2). \quad (12)$$

For long lag times  $\tau \gg \tau_0$ , the spatial probability distribution of the particle remains bounded, and the MSD converges towards a characteristic plateau value at  $\tau \rightarrow \infty$ :

$$R_b^2 = \overline{\Delta R^2}(\tau \rightarrow \infty) = 2\Gamma_w/(k_w\alpha). \quad (13)$$

In the following, the quantity  $R_b$  is called binding range. Note that  $R_b^2$  is inversely proportional to the stiffness  $k_w$  of the elastic well. The diffusion constant can also be expressed as

$$D = R_b^2/\tau_0. \quad (14)$$

Figure 4(a) compares the analytic expression (solid line) for the MSD (in units of  $R_b^2$ ) versus lag time (in units of  $\tau_0$ ) with a numerical simulation (symbols). The parameters have been chosen arbitrarily, so that  $\tau_0 = 100$  s and  $R_b^2 = 100 \mu\text{m}^2$ . The turning angle distributions, plotted in Fig. 4(b), show that complete inversions of the propagation direction become increasingly likely for lag times larger than the binding time  $\tau_0$ .

We can thus conclude that a superdiffusive MSD ( $b > 1$ ) corresponds to directional correlation of the bead motion and a subdiffusive MSD ( $b < 1$ ) is linked with directional anticorrelation. This close connection between diffusivity and directionality is a general property of random walks and can also be demonstrated analytically in some simple models [18,19].

### B. Effect of well center drift

In the previous section the particle performed a random walk in a static potential ‘‘landscape,’’ in our case given by a simple parabolic well. We now turn to a situation where this

<sup>3</sup>In  $n$ -dimensional space, the diffusion constant  $D$  is conventionally defined by the relation  $\langle \Delta R^2 \rangle = n2D\tau$ .

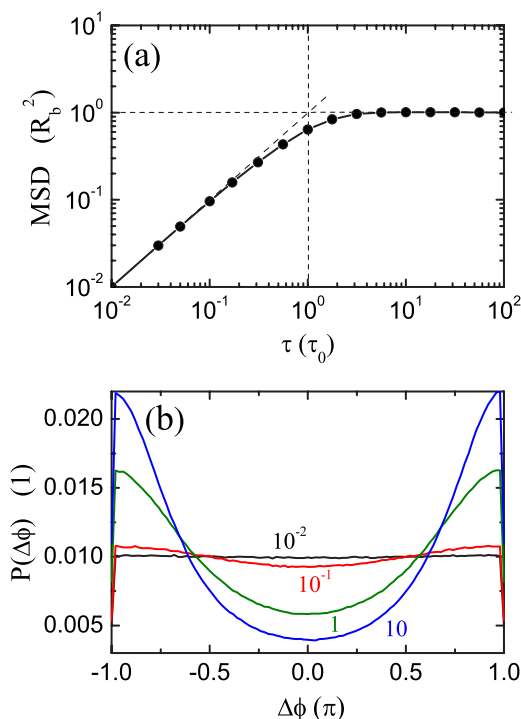


FIG. 4. (Color online) Diffusion in a potential well: (a) mean-square displacement (line, analytic solution; symbols, numerical simulation). The dashed line has a power-law exponent of 1. (b) Turning angle distributions for various lag times in units of  $\tau_0$ , showing increasingly antidiagonal behavior.

landscape is itself deforming slowly, i.e., on a long time scale compared to the characteristic time  $\tau_0$ . Such a gradual deformation can be modeled by continuous changes of the potential well parameters  $k_w$  and  $\vec{R}_{ctr}$ . In the following we focus on the possibility of a drifting well center  $\vec{R}_{ctr}(t) = \vec{e}v_w t$ , i.e., a ballistic motion of the center along direction  $\vec{e}$  with constant velocity  $v_w$ . A biophysical interpretation of such behavior is presented below. Note that an additional force acting on the bead, increasing linearly with time, is required to shift its equilibrium position with constant velocity.

The slow drift of the well center can have a significant effect on the particle within the well only for long enough lag times  $\tau > \tau_1$ . The characteristic time  $\tau_1$  is estimated by equating the distance  $v\tau_1$  which the center traveled ballistically with the binding range  $R_b$ . This yields

$$\tau_1 = R_b/v_w = \sqrt{2\Gamma_w/(k_w\alpha)}/v_w. \quad (15)$$

It is convenient to prescribe  $\tau_1$  instead of  $v_w$ . We assume here the relation  $\tau_0 < \tau_1$ . Let us finally note that in order to describe the essential experimental features, the drifting well model requires four generic parameters  $\alpha$ ,  $\Gamma_w$ ,  $k_w$ , and  $v_w$ .

We performed a computer simulation of particle diffusion in a harmonic well with random directed center motion for the parameters  $\alpha = 1$  pN s/ $\mu\text{m}$ ,  $R_b^2 = 100 \mu\text{m}^2$ ,  $\tau_0 = 10^1$  s, and  $\tau_1 = 10^4$  s.

Figure 5(a) shows that for lag times  $\tau > \tau_1$  the MSD is rising again from the plateau, reaching a superdiffusive local

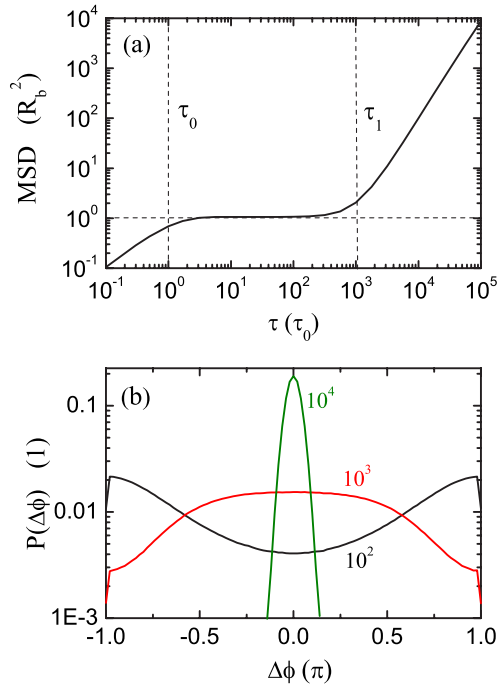


FIG. 5. (Color online) Effect of center drift. (a) Mean-square displacement. (b) Turning angle distributions for various lag times in units of  $\tau_0$ : transition from antidiagonal to directional behavior.

power-law exponent of two. The corresponding transition from “anticorrelated” to “correlated” turning angles at times around  $\tau_1$  can be clearly seen in Fig. 5(b).

In the present generic model, the characteristic times  $\tau_0$  and  $\tau_1$  define up to three distinct regimes. With respect to the experimental findings to be explained, however, our focus lies in the subdiffusive to superdiffusive transition at  $\tau_1$ , with its associated changes of directionality. We consider the “plateau regime” and the subsequent “traction regime” as essential and robust properties of the model. Other features, like the behavior at extreme lag times ( $\tau < \tau_0$  and  $\tau \gg \tau_1$  lag times (being not accessible with our current experimental setup), depend more sensitively on the detailed assumptions made and are thus considered secondary for this paper.<sup>4</sup>

<sup>4</sup>It should be noted that other groups, investigating different systems and using faster experimental techniques such as laser tracking, have reported data which could be used as evidence for the subdiffusive regime  $\tau < \tau_0$ . For instance, Yamada *et al.* [4] observed a gradual transition from diffusive MSD to a plateau even for thermally driven polystyrene beads in gelatin. Tolic-Norrelykke *et al.* [20] investigated the fluctuations of lipid granules in living yeast cells and found subdiffusive behavior with a power-law exponent of around 0.75 in the lag time regime from  $10^{-4}$  to 10 s. Their data provide, however, only weak evidence for the onset of a plateau. Nevertheless, also the theory of semiflexible polymer networks predicts for long lag times a plateau in the MSD due to elastic trapping [21]. In the regime of extremely long times,  $\tau \gg \tau_1$ , where the whole structure of the cytoskeleton can be remodeled drastically, processes like cell crawling already start to play a role. Such effects are beyond the scope of our simple model.

## VI. BIOPHYSICAL MODEL

Next we present a biophysical realization of the generic model of a drifting well. Our basic assumption is that the bead (representing the particle) becomes a node in a network of dynamically remodeling stress fibers. These ATP-powered acto-myosin fibers have the multiple roles of (I) providing the rapid force fluctuations, (II) of creating an elastic potential well, (III) of generating force ramps during their development, and (IV) of producing a constant level of prestress afterwards. The details of the model are described in the following sections.

### A. Cell and bead

Because it is the bead that we directly observe in the experiments, it forms the central object of our model. Due to its fibronectin coating, the bead becomes an integrated part of the cytoskeleton.

We assume a cell of flat shape, adhering strongly to a relatively rigid substrate underneath. Our model is effectively two dimensional, with a disk-shaped bead floating in a continuous, viscous, intracellular background fluid. We do not consider further geometric details such as partial or complete internalization of the bead into the cell. Since the cytosol is crowded with soft matter, the background viscosity is chosen to be rather high [22]. In Ref. [5], the rheological response of the average cellular medium has been determined to be a weak power law (here attributed to the fiber network), with a superimposed linear background viscosity of 1.4 Pa s (in this paper attributed to the cytosolic background fluid). Neglecting friction contributions due to the dragging of the fiber network through the cytosol, the friction constant  $\alpha$  can be estimated by the three-dimensional (3D) Stokes formula

$$\alpha = 6\pi\eta r_{\text{bead}}. \quad (16)$$

While the cytosol causes only damping of the bead motion and energy dissipation, the most important part of the model cell is the cytoskeleton, a connected meshwork of semiflexible polymer filaments and cross linkers. A part of the filaments is connected to trans-membrane receptors (FAs) and thereby anchored to the substrate. Another part of filaments is mechanically coupled to FAs forming on the surface of the suitably coated bead.

### B. Fiber network topology

In the cytoskeletal network we distinguish passive filaments (without working motor proteins) and active fibers (creating internal forces), called stress fibers. For simplicity, we ignore the passive filaments altogether and focus on those stress fibers directly attached to the bead. For a bead of given size, the maximum number of direct stress fibers is limited by steric hindrance. We postulate here a constant average number of  $N_f$  fibers. Attached fibers project radially outward from the bead center and have (at the time of first formation) an average length  $L_f$ . This leads to a “spider web”-shaped geometry of the network in the immediate vicinity of the bead (compare to Fig. 6). A realistic modeling of the com-

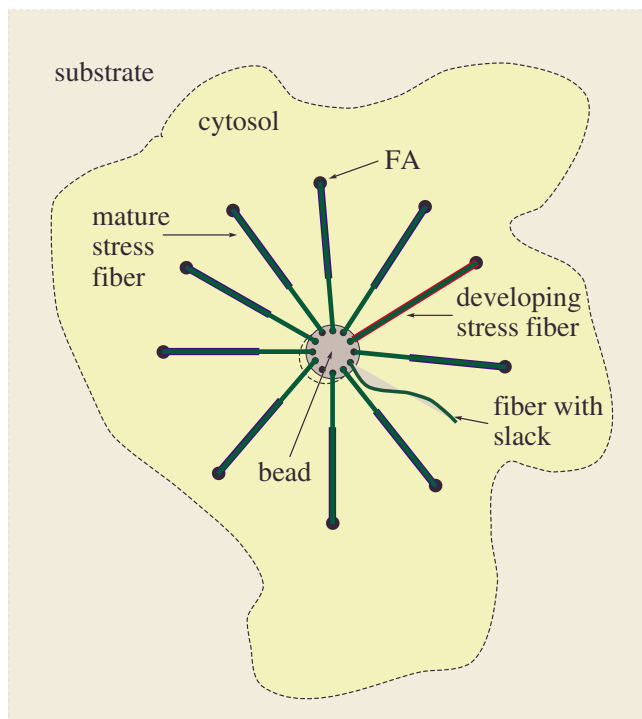


FIG. 6. (Color online) Schematic “spider” network, showing fibers in various stages of their development.

plete fiber network is beyond the scope of this paper. We simply assume here that the remote end of each direct stress-fiber is tightly anchored to the substrate via a *trans*-membrane FA (rather than being cross-linked to the distant parts of the network).

### C. Collective fiber properties

We first ignore the internal biomechanical structure of real stress fibers and use a minimalistic “black box model” that provides just the essential features: elasticity and force fluctuations, as well as a growing and finally saturating prestress. The temporal development of the fiber is schematically drawn in Fig. 7. The time of birth,  $t=0$ , occurs when both ends of the fiber are firmly attached to focal adhesions and the fiber has shrunk enough to remove any initial slack. From then on, the fiber will affect the bead motion.

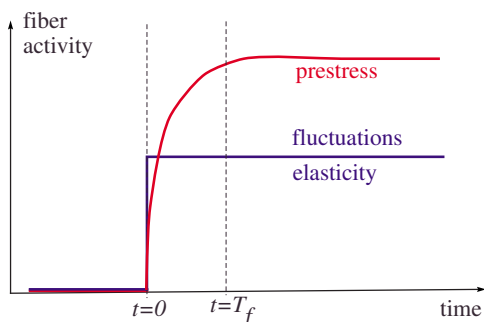


FIG. 7. (Color online) Development of the model fiber.

In particular, we assume that the fiber generates along its momentary direction white noise force fluctuations of power spectral density  $\Gamma_f$ . In addition, it acts as a Hookian spring of stiffness  $k_f$ . This model describes the stress fiber as a homogeneous elastic cylinder of length  $L_f$  and radius  $r_f$ , we can relate the spring constant  $k_f$  to a collective elastic modulus  $E_f$  via

$$k_f = F/\Delta L = (\pi r_f^2)E_f/L_f. \quad (17)$$

At given momentary length  $L(t)$  and rest length  $L_{rest}(t)$ , the resulting elastic force is

$$F(t) = k_f[L(t) - L_{rest}(t)]. \quad (18)$$

At the time of birth, we set  $L(0) = L_{rest}(0) = L_f$ . From then on, the rest length is shrinking<sup>5</sup> in proportion to a developmental variable  $\lambda(t) \in [0, 1]$ , according to

$$L_{rest}(t) = L_0 - (F_f/k_f)\lambda(t). \quad (19)$$

Here,  $F_f$  is the maximum (asymptotic) force the fiber would produce under isometric conditions. We first consider a simple transient dynamics, according to

$$\lambda(t) = 1 - e^{-t/T_f}. \quad (20)$$

This produces a growing and eventually saturating prestress, as shown in the figure. Here,  $T_f$  is the fiber buildup time. For small times compared to  $T_f$ , we have  $\lambda(t \ll T_f) = t/T_f$ . If  $L(t)$  were fixed, the fiber prestress force would in this transient regime increase linearly at a rate  $\dot{F}_f = F_f/T_f$ .

<sup>5</sup>The shrinking of the fiber’s rest length should be considered as a macroscopic net effect of complex biophysical and biochemical processes on the microscopic level. For a simple picture, imagine a minimalistic stress fiber model, consisting of just two straight and parallel actin filaments, one end of each filament being connected to a focal adhesion. If the sum of the filament lengths exceeds the distance between the adhesions, there is a region of mutual filament overlap where myosin motors can cross-link and create traction forces. In the case where both adhesion positions are rigidly fixed to the substrate (isometric conditions), the filaments would thereby become slightly stretched and the system would quickly reach a new equilibrium configuration. On somewhat longer time scales, the actin filaments can grow longer by continuous polymerization at their open ends. As a result, the zone of overlap increases and additional myosin molecules find opportunities to cross-link. In reality, the actual number and activity of the myosins, as well as the rates of actin polymerization or depolymerization, can be regulated by complex biochemical control networks, which also involve the focal adhesions. In our model, one of the focal adhesions is connected to the viscoelastically bound bead and is therefore mobile to a certain extent. While the mobile adhesion is pulled towards the fixed one by the fiber’s self-created tension, the parallel filaments can perform a sliding motion similar to muscle filaments. Under such dynamic conditions, the average force produced by the collective myosin activity is expected to be reduced, as compared to the static situation. In the present model, we subsume all those effects into a “developmental parameter”  $\lambda(t)$ , while quantities such as the number of myosins  $N_m$  in the fiber, or the maximum force  $F_f$  which they can produce, are considered to be constant.

#### D. Acto-myosin model

This section relates the collective fiber properties  $F_f$  and  $\Gamma_f$  to the microscopic parameters of the acto-myosin system. In the simplest microscopic model, a stress fiber consists of actin filaments, which are dynamically cross-linked by myosin motor proteins (as well as other types of linked molecules not considered here). It is assumed that each myosin molecule repeatedly attaches to a pair of actin filaments for a period  $\tau_m$ , during which it produces a constant force  $f_m$  in the fiber. The cycle time  $T_m$  between two successive attachments is fluctuating according to Poisson statistics, with an average  $\bar{T}_m$ . The duty ratio of the myosin motor is therefore  $\epsilon_m = \tau_m/\bar{T}_m$ . Let there be  $N_m$  myosin molecules in the fiber, acting statistically independently and additively.<sup>6</sup>

Then, the average force per myosin is given by  $\bar{f}_m = \epsilon_m f_m$  and the total force of the fiber by  $F_f = N_m \bar{f}_m = N_m \epsilon_m f_m$ . The transient growth rate of the fiber force is

$$\dot{F}_f = N_m \epsilon_m f_m / T_f. \quad (21)$$

The power spectrum of the force fluctuations can be derived in this simple model as follows: We describe the individual force pulse of a myosin during attachment as  $a_m(t) = f_m \text{box}_{\tau_m}(t)$ , where  $\text{box}_{\tau_m}(t) = 1$  for  $t \in [-\tau_m/2, +\tau_m/2]$  and  $\text{box}_{\tau_m}(t) = 0$  otherwise. The successive reattachment events are expressed as a sequence of  $\delta$ -peaks,  $p_m(t) = \sum_{k=1}^n \delta(t - t_{mk})$ , with  $n \rightarrow \infty$ . The intervals  $T_{mk} = t_{mk} - t_{mk-1}$  are Poisson distributed with mean  $\langle T_{mk} \rangle_k = \bar{T}_m$ . The pulse train of forces due to a single myosin is the convolution  $f_m(t) = p_m(t) \otimes a_m(t)$ . Its Fourier transform  $f_m(\omega)$  is related to the power spectrum:  $S_m(\omega) = \frac{1}{n\bar{T}_m} |f_m(\omega)|^2 = \left( \frac{1}{n\bar{T}_m} |p_m(\omega)|^2 \right) |a_m(\omega)|^2$ . The term in brackets is the spectral power of the infinite sequence of  $\delta$  peaks and equals the rate of the Poisson process, i.e.,  $1/\bar{T}_m$ . The Fourier transform of the single force pulse is  $a_m(\omega) = f_m \tau_m \text{sinc}(\omega \tau_m / 2)$ , with  $\text{sinc}(x) = \sin(x)/x$ . The PSDs of the  $N_m$  myosins are additive, so that  $S_f = N_m S_m$ . In the long-time (small-frequency) limit  $\omega \ll (1/\tau_m)$ , the sinc function is  $\approx 1$ , the spectrum is flat, and the effective white noise power spectral density (PSD) of the fiber is given by the prefactors,  $\Gamma_f = S_f(\omega=0)$ , and thus

$$\Gamma_f = N_m f_m^2 \tau_m \epsilon_m. \quad (22)$$

#### VII. RELATING THE BIOPHYSICAL AND DRIFTING WELL MODELS

In this section, we will map the collective biophysical properties onto the four generic quantities characterizing the drifting well model. As the friction constant  $\alpha$  is common to both models, the only task is to compute the collective well

<sup>6</sup>This is a simplifying assumption. In reality, a part of the myosin motors within the fiber might work in opposite directions. Another part might be inactive. Therefore,  $N_m$  should be interpreted as the effective number of myosin motors which actually contribute to the fiber contraction.

properties  $\Gamma_w$ ,  $k_w$ , and  $v_w$  from those of the  $N_f$  individual fibers. For this end, we assume that in the statistical average, the fiber directions will be isotropic with respect to the well center.

Due to the isotropy, the elastic well formed by the radial fibers behaves as a harmonic potential well for small deviations from the minimum position. (Note that the prestress existing in the fibers does not affect its elastic properties in our linear model.) The collective isotropic stiffness  $k_w$  of the well can be estimated by considering a small bead deviation  $\Delta x$  from the minimum towards the  $x$  direction. The total ( $x$  component of the) binding force is the sum of elastic forces exerted by the individual fibers. In the limit of long fibers, the component contributed by a fiber in orientation  $\theta$  is  $F_\theta = k_f \Delta x \cos^2 \theta$ . The average isotropic stiffness of the well is therefore given by

$$k_w = N_f k_f \langle \cos^2 \theta \rangle = (1/2) N_f k_f. \quad (23)$$

Another function of the fibers is the generation of force fluctuations. Since each fiber fluctuates independently with power density  $\Gamma_f$  along its direction  $\theta$ , the variances of the random force components are additive. The total random forces on the bead in the  $x$  and  $y$  directions remain uncorrelated. On average, accounting again for the  $\cos \theta$  factors, one obtains

$$\Gamma_w = (1/2) N_f \Gamma_f. \quad (24)$$

Finally we have to estimate the well drift velocity  $v_w$  from the well stiffness  $k_w$  and the force growth rate  $\dot{F}_f$  of the  $N_f$  fibers. An individual fiber would shift the well center with velocity  $v_1 = \dot{F}_f / k_w$  along the fiber direction. These individual velocities add up linearly. Assuming independent velocity vectors with random directions and performing a statistical average, one obtains for the absolute value of the resulting sum velocity  $v_w = (\sqrt{\pi/4} \sqrt{N_f}) v_1$ , and therefore

$$v_w = \sqrt{\frac{\pi}{4}} N_f \frac{\dot{F}_f}{k_w}. \quad (25)$$

#### VIII. EXTRACELLULAR MATRIX FLUCTUATIONS

The central assumption of this work is that fibroectin-coated beads report fluctuations of the cytoskeleton, and not (or only to a much smaller extent) those of the cytosol. Since the firm connection of the beads to the actomyosin network is usually not immediately apparent by optical observation, it is essential to confirm our assumption by other means. For this purpose, we have shown in our experimental paper [12] that the intracellular random motion of the coated beads is highly correlated with the motion of markers in the elastic extracellular matrix (ECM), to which the cytoskeleton is attached via focal adhesions at the basal side of the cell. We will derive in the following the statistical properties of the extracellular marker fluctuations.

In our simplified network model, the remote end of each stress fiber is anchored to the substrate beneath the cell. We treat this substrate as a homogeneous, linear elastic half

space with Poisson ratio  $\sigma$  and Young's modulus  $Y$ , much stiffer than the fiber network. The forces acting in the stress fiber network will then cause small, time-dependent deformations of the substrate, which can be monitored experimentally by measuring the spatial shifts of markers attached to the substrate (traction microscopy).

The shift of a marker at the origin due to single localized traction force  $\vec{F}$  applied at position  $\vec{r}=(x,y)$  is provided by the Boussinesq solution [23]:

$$\Delta\vec{R}_M = \mathbf{K}(\vec{r})\vec{F}, \quad (26)$$

where the matrix Green's function  $\mathbf{K}(\vec{r})$  is given by

$$\mathbf{K}(\vec{r}) = \left(\frac{1+\sigma}{\pi Y}\right) \frac{1}{r^3} \begin{bmatrix} (1-\sigma)r^2 + \sigma x^2 & \sigma xy \\ \sigma xy & (1-\sigma)r^2 + \sigma y^2 \end{bmatrix}. \quad (27)$$

The positions of the substrate-bound FAs are denoted by  $\vec{R}_s$ , the marker position by  $\vec{R}_M$ , and the difference vectors by  $\vec{r}_s = \vec{R}_M - \vec{R}_s$ . The shift of the marker is then the linear superposition of the individual stress fiber contributions:

$$\Delta\vec{R}_M = \sum_{s=1}^{S_{\max}} \mathbf{K}(\vec{r}_s)\vec{F}_s. \quad (28)$$

Because the Green's function decays as  $1/r$ , only markers in the near vicinity of at least one FA show appreciable fluctuations. Since the typical distances between the FAs is large (assuming the spiderweb geometry with a modest number of rather long fibers), the motion of those significant markers is dominated strongly by the single contribution of their nearby FA. We can therefore assign only one marker to each FA and denote it by the same index  $s$ . The displacement of marker  $s$  directly reflects the individual stress fiber force  $\vec{F}_s$ . Note that this is in contrast to the case of the intracellular bead, which always "feels" the equally weighted sum of all the attached stress fibers.

The marker follows the stress fiber force instantaneously, because it is attached to a purely elastic medium. In contrast to the bead (which is part of a viscoelastic medium and thereby moves diffusively for very short lag times  $\tau < \tau_0$ ) the marker has a relaxation time  $\tau_0$  close to zero. We thus expect for the marker MSD a plateau extending to very short lag times.

## IX. CHOICE OF PARAMETERS

Next we present and motivate our choice of the model parameters. The subset of experimental data which is compatible with the drifting well model, i.e., the MSD traces which show an extended plateau of slope  $\approx 0$  and a superdiffusive regime with slope  $\approx 2$ , can be characterized by only three values: the binding time  $\tau_0$  (actually, only an upper limit is provided experimentally), the binding range  $R_b$ , and the transition time  $\tau_1$ . On the other hand, we have a total of 11 microscopic model parameters for the acto-myosin system, the stress fibers as a whole, the bead, and the cytosole. There should consequently exist a 8-dimensional parameter

subspace which is compatible with the 3 experimental key quantities. However, for almost all of the 11 model parameters a range of reasonable values can be extracted from the literature. Within those rather narrow constraints, the "fitting" of the model to the data becomes nontrivial.

The analytic mapping of the biophysical model onto the four drifting well properties also allows for independent tests: For example, the collective stiffness of the well (fiber network) can be measured separately by active microrheology. In the following, comments on the various quantities are presented as footnotes.

The microscopic model parameters are as follows:

Parameter	Unit	Fit	Ref. val.	Ref./Com
Myosin pulse force	$f_m$	pN	1	1–5 [24]
Myosin pulse width	$\tau_m$	ms	0.1	0.1–1 [25]
Myosin duty cycle	$\epsilon_m$	1	1	0.8–1 [26]
Myosins per fiber	$N_m$	1	$10^4$	( $10^4$ ) [27]
Fiber length	$L_f$	$\mu\text{m}$	10	14 [29]
Fiber radius	$r_f$	$\mu\text{m}$	0.1	0.1–0.25 [16]
Fiber Young mod.	$E_f$	kPa	100	1450–632 [30]
Fiber buildup time	$T_f$	s	$10^3$	>200 [31]
Fibers per bead	$N_f$	1	10	<50 [32]
Bead radius	$r_{\text{bead}}$	$\mu\text{m}$	2	2 [12]
Cytos. viscosity	$\eta$	Pa s	2	1.4 [5]

Using the microscopic parameters from above, we can compute the collective properties of single stress fibers and the friction of the bead in the background cytosol:

Property	Unit	Val.	Com.
Friction constant	$\alpha$	pN s/ $\mu\text{m}$	37.7 Eq. (16)
Fiber stiffness	$k_f$	nN/ $\mu\text{m}$	0.314 Eq. (17)
Fiber noise PSD	$\Gamma_f$	nN <sup>2</sup> $\mu\text{s}$	1 Eq. (22)
Fib. force growth rate	$\dot{F}_f$	pN/s	10 Eq. (21)

Finally, the resulting characteristic quantities of the drifting well model are as follows:

Quantity	Unit	Val.	Com.
Friction constant	$\alpha$	pN s/ $\mu\text{m}$	37.7 Eq. (16)
Well stiffness	$k_w$	nN/ $\mu\text{m}$	1.57 Eq. (23) [33]
Well noise PSD	$\Gamma_w$	nN <sup>2</sup> $\mu\text{s}$	5 Eq. (24) [35]
Well velocity	$v_w$	nm/s	17.9 Eq. (25) [36]

## X. RESULTS AND DISCUSSION

### A. Intracellular bead motion

We next discuss the simulation results of the biophysical model [solid lines in Figs. 8(a)–8(c)] and compare them directly to experimental data (symbols).

Figure 8(a) shows the MSD versus lag time. The simulation was based on the microscopic model parameters as pre-

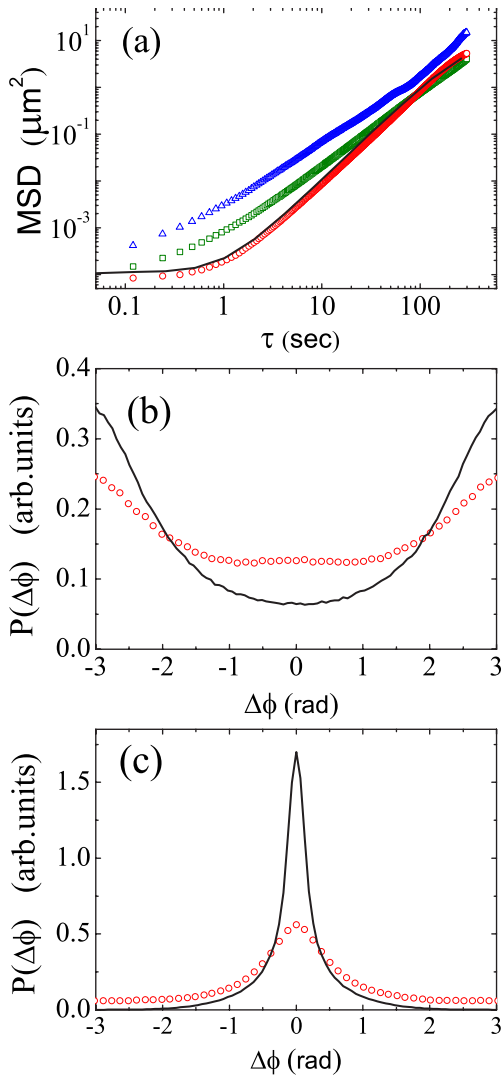


FIG. 8. (Color online) Comparison of simulation results (solid lines) with experimental data (symbols). (a) MSD versus lag time for the bead motion. Spheres: samples with a pronounced plateau. Squares: ensemble average. Triangles: samples without a plateau. (b),(c) Turning angle distributions for lag times of 0.1 s and 10 s, respectively.

sented above. Note that our fit was aimed at the subclass of experimental trajectories which show a clear plateau as well as a ballistic regime. In this case (spherical symbols) the agreement is nearly perfect. However, the experimental data also contained almost purely diffusive trajectories (triangular symbols), as well as intermediate cases. We presume that such behavior is due to beads that have bound not at all, or not permanently, to the stress fiber network.<sup>7</sup> The average over all measured MSD traces (performed in double-

<sup>7</sup>One could imagine a scenario where the bead repeatedly couples and decouples from the network associated with diffusive and ballistic phases of motion. In a different context, it has been shown [37] that such a two-phase stochastic process can exhibit a power law MSD with fractional exponent. This is actually observed in some of our experimental trajectories.

logarithmic representation) is plotted with quadratic symbols.

Figure 8(b) shows the turning angle distributions at a lag time of 0.1 s, and Fig. 8(c) at 10 s. The theory reproduces the characteristic transition from antipersistent (b) to persistent (c) behavior, but overestimates the degree of antipersistence (persistence) at very short (long) lag times.

### B. Alternative remodeling dynamics

In the model described so far, we have assumed that the prestress generated by the fibers increases linearly at small times and finally saturates. This simple choice was sufficient to reproduce the experimental data. However, it is quite unrealistic that all fibers run through the same developmental curve  $\lambda(t)$ , simultaneously and without any individual parameter fluctuations. Also, this model describes transient behavior and not a stationary random process, as is usually assumed when a MSD is computed.<sup>8</sup> Biologically, we would rather expect each fiber to develop independently from the others. In addition, it will not remain in the mature state forever, but be remodeled on long time scales. It is therefore instructive to investigate the effect of a more complex remodeling dynamics on the general characteristics of the MSD. The main purpose of this section, however, is to clarify which features of the fiber dynamics are essential for reproducing the data and which have no detectable effect on the MSD or TAD. In particular, it will be demonstrated that mutually independent, but long-time persistent fluctuations of the fiber forces are sufficient.

Figure 9(a) shows a case of oscillatory dynamics, described by a developmental parameter

$$\lambda_k(t) = \frac{1}{2} + \frac{1}{2} \sin\left(\phi_k + 2\pi \frac{t}{T_k}\right). \quad (29)$$

The phase shifts  $\phi_k$  were chosen randomly for each fiber, equally distributed between 0 and  $2\pi$ . To avoid periodic dynamics, which would lead to a periodic MSD versus lag time, the individual remodeling periods  $T_k$  where also equally distributed between  $\frac{1}{2}T_0$  and  $\frac{3}{2}T_0$ . We used a long average period  $T_0$  of 1000 s. The result (line with quadratic dots) shows the same basic features as our original transient model (plotted with a dashed line). This demonstrates that only the long-time persistence of the forces is required to move an elastically bound bead with constant velocity.

In Fig. 9(b) we explore the effect of a prestress with correlated Gaussian fluctuations around some average value. (The white noise of the PSD  $\Gamma_w$  was additionally present in the following simulations.) The developmental parameter was chosen as

$$\lambda_k(t) = \bar{\lambda} + \Delta\lambda_k(t), \quad (30)$$

where the random processes  $\Delta\lambda_k$  were Gaussian distributed with variance  $\sigma^2$ —i.e.,  $P(\Delta\lambda) \propto e^{-(1/2)\Delta\lambda^2/\sigma^2}$ —and had an exponentially decaying temporal correlation with time constant  $\tau_c$ —i.e.,  $\langle \Delta\lambda(t)\Delta\lambda(t') \rangle = \sigma^2 e^{-|t-t'|/\tau_c}$ . (Note that this correlated

<sup>8</sup>For a transient process, even the ensemble-averaged MSD will depend on the absolute time  $t$ , in addition to the lag time  $\tau$ .

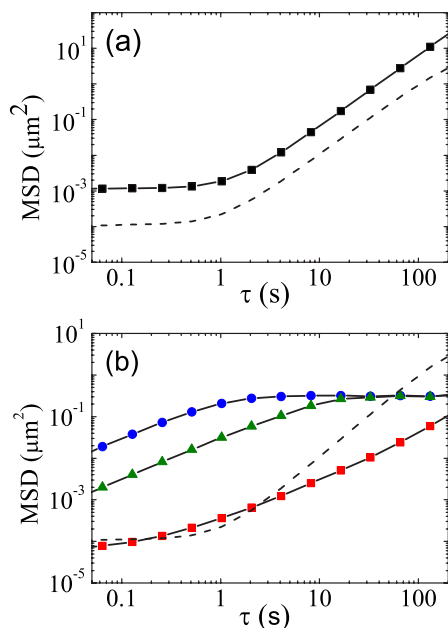


FIG. 9. (Color online) MSD versus lag time for alternative remodeling dynamics. The dashed lines repeat the theoretical result from Fig. 8(a), corresponding to the transient case. (a) Oscillatory dynamics. (b) Correlated Gaussian fluctuations, for three different correlation times  $\tau_c=1$  s (spheres),  $\tau_c=10$  s (triangles), and  $\tau_c=1000$  s (squares).

noise has a Lorentzian power spectrum with rollover time  $\tau_c$ . For longer lag times, it becomes effectively white. It therefore qualitatively resembles the noise of ATP-powered motor proteins.)

As shown in Fig. 9(b), the resulting MSD grows approximately diffusive for  $\tau < \tau_c$  and saturates for all longer lag times. For the longest correlation time  $\tau_c=1000$  s (square symbols), where the white “background noise” starts to dominate, a subdiffusive regime appears at small lag times. Nevertheless, the overall curve is not compatible with the measurements. We conclude that the MSD features observed in the experiments cannot be explained by a fluctuating prestress with finite correlation time  $\tau_c$ , but require long-time persistent forces.

### C. Extracellular marker motion

Based on the analysis of Sec. VIII, we directly monitored the force  $\vec{F}_k$  which the  $k$ th stress fibers exerts on its focal adhesion. By introducing an effective isotropic elastic stiffness  $k_{eff}$ , we defined displacements  $\Delta\vec{R}_k = \vec{F}_k / k_{eff}$ . The value of  $k_{eff}$ , reflecting a combination of the stiffnesses of the substrate and of the focal adhesion contact, was chosen to fit the experimental data. The other simulation parameters were identical to the case of intracellular bead motion. Note that  $\Delta\vec{R}_k$  can be interpreted as the displacement of the focal adhesion itself, relative to its unstrained position  $\vec{R}_k$  in the substrate.

Based on the fluctuations of  $\Delta\vec{R}_k$ , we computed a MSD versus lag time, as plotted in Fig. 10. For this simulation, we

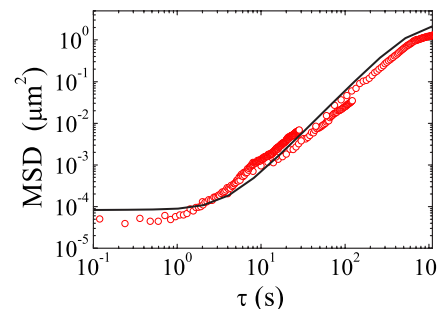


FIG. 10. (Color online) MSD versus lag time for the markers in the ECM. Symbols: experiment. Solid line: theory.

used the oscillatory remodeling dynamics, as described above, however with an average remodeling period  $T_0$  of 3000 s. The effective stiffness  $k_{eff}$  was 5 nN/ $\mu$ m.

We note that the predicted, extended plateau at small lag times is clearly visible in the experiment. On extremely long time scales, even the persistent prestress fluctuations can be viewed as noise. We therefore expect an additional asymptotic plateau in the marker MSD. The data show the onset of this feature.

## XI. SUMMARY AND OUTLOOK

The MSD of cytoskeleton-bound beads show a subdiffusive to superdiffusive transition, accompanied with characteristic features of the turning angle distributions, indicating a change from antipersistent to persistent motion. In this paper, we have interpreted this transition as a crossover between a flat and a steep power law, driven by noise and persistent forces, respectively.

The generic physics of the system corresponds to the diffusion of a particle within a slowly drifting potential well. As a concrete biophysical model we proposed that the bead becomes a node in a dynamically remodeling network of stress fibers. The collective properties of these fibers, such as elasticity, force fluctuations, and maximum average force, have been analytically estimated from a simple microscopic model of the acto-myosin system. Choosing the microscopic parameters from within the narrow range of experimentally confirmed (or at least reasonable) values, quantitative agreement with the data was achieved, for both beads bound to the cytoskeleton and markers in the ECM.

Our model was based on several simplifying assumptions. For example, we assumed an elastic fiber network submerged in a viscous cytosol. However, active microrheology shows that the cytoskeleton is not purely elastic, but has a weak power-law response. First numerical simulations using this realistic response function (not presented here) indicate that the “horizontal” plateau in the MSD is then replaced by a subdiffusive power-law regime with a small exponent. This agrees with some of the measured MSD traces. Yet further work is required to separate the contributions from colored noise and from the complex response function.

Also, we aim to develop a more refined microscopic model of the stress fibers, possibly resembling Huxley’s sliding filament model of the muscle. A direct numerical simu-

lation of the dynamic cross bridge activity will provide a detailed understanding of the average prestress produced in each fiber and its temporal fluctuations, in particular under realistic conditions of slow filament sliding.

In the present model, different possible remodeling dynamics were chosen “by hand.” As it turned out, the only important factor to produce a ballistic regime in the MSD is a sufficient degree of temporal persistence in the prestress development. A realistic description of the fiber network’s long-time remodeling will have to include processes such as focal adhesion formation, actin polymerization, and depolymerization, myosin activation, as well as the biochemical pathways controlling that behavior.

Future theoretical work could also include model extensions that provide a MSD with a broad power-law regime and fractional exponent, as observed experimentally. This can be achieved, for instance, with a more detailed model of focal adhesion formation, yielding fat-tailed distributions of rupture lifetimes for the connected actin fibers.<sup>9</sup>

Even without these refinements, our model of cytoskeletal fluctuations will help biologists to extract quantitative information on cytoskeletal structure and dynamics from simple bead diffusion experiments.

#### ACKNOWLEDGMENTS

This work was supported by the Deutsche Forschungsgemeinschaft, the Deutsche Krebshilfe, and the National Institutes of Health, Grant Nos. MA 534/20-4, 107384, and HL65960.

#### APPENDIX: DIFFUSION IN A HARMONIC WELL

We consider a particle diffusing within an isotropic elastic well of stiffness  $k$ , centered at the origin  $\vec{R}_{ctr} = \vec{0}$ . The potential well  $U = (k/2)R^2$  produces a binding force  $F^{(ela)}(\vec{R}) = -k\vec{R}$ , so that

$$\vec{F}^{(tot)} = \vec{F}^{(rnd)} + \vec{F}^{(fri)} + \vec{F}^{(ela)}. \quad (\text{A1})$$

The equation of motion can be written in the form

<sup>9</sup>As one of the possible scenarios, one can envision fibers which are continuously building up a growing prestress (translated into directed motion of the bead), until their life ends prematurely by rupture of the focal adhesion. If such yielding events follow Bell kinetics and, if the rupture forces are exponentially distributed around an average value  $\bar{F}_{rup}$ , one obtains a tunable MSD exponent with a fractional value set by  $\bar{F}_{rup}$  (a mechanism similar to that used in [9]). The exponential distribution of rupture times, in turn, could be explained by the kinetics of the focal adhesion formation, when an increasing number of parallel load-bearing elements are added to the complex at constant rate, until the reinforcement is suddenly terminated by some (perhaps biochemical) event with Poisson arrival time statistics.

$$\left[ \alpha \frac{d}{dt} + k \right] \vec{R}(t) = \vec{F}^{(rnd)}(t). \quad (\text{A2})$$

The response (Green’s) function  $G(t)$  of this linear system is the special solution of the above equation for a  $\delta$ -like driving force pulse:

$$\left[ \alpha \frac{d}{dt} + k \right] G(t) = \delta(t - 0). \quad (\text{A3})$$

It is given by

$$G(t) = \frac{1}{\alpha} \theta(t - 0) e^{-(k/\alpha)t}, \quad (\text{A4})$$

where  $\theta(t)$  is the Heaviside step function. The trajectory resulting from a general random force  $\vec{F}^{(rnd)}(t)$  is then the convolution  $\vec{R}(t) = G(t) \otimes \vec{F}^{(rnd)}(t)$  or

$$\vec{R}(t) = \frac{1}{\alpha} \int_{-\infty}^t dt' e^{-(k/\alpha)(t-t')} \vec{F}^{(rnd)}(t'). \quad (\text{A5})$$

To determine the statistical properties of the particle trajectory, we consider the correlator

$$c(\tau) = \langle \vec{R}(\tau) \vec{R}(0) \rangle = \int_{-\infty}^{\tau} dt_1 \int_{-\infty}^0 dt_2 e^{-(k/\alpha)(\tau-t_1-t_2)} \langle \vec{F}^{(rnd)}(t_1) \vec{F}^{(rnd)}(t_2) \rangle / \alpha^2. \quad (\text{A6})$$

We assume that the random force is isotropic white noise on the time scale considered here:

$$\langle F_i^{(rnd)}(t) F_j^{(rnd)}(t') \rangle = \delta_{ij} \Gamma \delta(t_1 - t_2), \quad (\text{A7})$$

where  $\Gamma$  is the spectral power density of the noise in each spatial dimension. If the actual random force fluctuations have a variance  $\bar{F}^2$  and a small, but finite correlation time  $\tau_1$ , the effective noise density is  $\Gamma = 2\bar{F}^2\tau_1$ . The vectorial auto-correlation then reads

$$\langle \vec{F}^{(rnd)}(t_1) \vec{F}^{(rnd)}(t_2) \rangle = 2\Gamma \delta(t_1 - t_2). \quad (\text{A8})$$

Inserting this into Eq. (A6) yields for the spatial correlator

$$\langle \vec{R}(\tau) \vec{R}(0) \rangle = \frac{\Gamma}{k\alpha} e^{-(k/\alpha)\tau}. \quad (\text{A9})$$

Its value at zero lag time,  $c(0) = \langle R^2 \rangle = \frac{\Gamma}{k\alpha}$ , describes the variance of the spatial fluctuations relative to the origin of the coordinate system. The MSD can be easily computed from the above correlator using the relation

$$\begin{aligned} \overline{\Delta R^2}(\tau) &= \langle [\vec{R}(\tau) - \vec{R}(0)]^2 \rangle = 2(\langle R^2 \rangle - \langle \vec{R}(\tau) \vec{R}(0) \rangle) \\ &= \frac{2\Gamma}{k\alpha} (1 - e^{-(k/\alpha)\tau}). \end{aligned} \quad (\text{A10})$$

- [1] T. G. Mason and D. A. Weitz, *Phys. Rev. Lett.* **74**, 1250 (1995).
- [2] E. Frey and K. Kroy, *Ann. Phys.* **14**, 200410132 (2005).
- [3] V. Breedveld and D. J. Pine, *J. Mater. Sci.* **38**, 4461 (2003).
- [4] S. Yamada, D. Wirtz, and S. C. Kuo, *Biophys. J.* **78**, 1736 (2000).
- [5] B. Fabry, G. N. Maksym, J. P. Butler, M. Glogauer, D. Navajas, and J. J. Fredberg, *Phys. Rev. Lett.* **87**, 148102 (2001).
- [6] B. Fabry *et al.*, *J. Appl. Physiol.* **91**, 986 (2001).
- [7] J. Alcaraz *et al.*, *Biophys. J.* **84**, 2071 (2003).
- [8] M. Baland *et al.*, *Phys. Rev. E* **74**, 021911 (2006).
- [9] P. Sollich, F. Lequeux, P. Hebraud, and M. E. Cates, *Phys. Rev. Lett.* **78**, 2020 (1997).
- [10] A. W. C. Lau, B. D. Hoffmann, A. Davies, J. C. Crocker, and T. C. Lubensky, *Phys. Rev. Lett.* **91**, 198101 (2003).
- [11] P. Bursac *et al.*, *Nat. Mater.* **4**, 557 (2005).
- [12] C. Raupach *et al.*, *Phys. Rev. E* **76**, 011918 (2007).
- [13] M. L. Gardel, J. H. Shin, F. C. MacKintosh, L. Mahadevan, P. Matsudaira, and D. A. Weitz, *Science* **304**, 1301 (2004).
- [14] M. L. Gardel, F. Nakamura, J. Hartwig, J. C. Crocker, T. P. Stossel, and D. A. Weitz, *Phys. Rev. Lett.* **96**, 088102 (2006).
- [15] S. Kumar, I. Z. Maxwell, A. Heisterkamp, T. R. Polte, T. P. Lele, M. Salanga, E. Mazur, and D. E. Ingber, *Biophys. J.* **90**, 3762 (2006).
- [16] S. Deguchi, T. Ohashi, and M. Sato, *J. Biomech.* **39**, 2603 (2006).
- [17] A. Caspi, R. Granek, and M. Elbaum, *Phys. Rev. E* **66**, 011916 (2002).
- [18] N. Komin, U. Erdmann, and L. Schimansky-Geier, *Fluct. Noise Lett.* **4**, L151 (2004).
- [19] G. A. Dunn, *Agents Actions Suppl.* **12**, 14 (1983).
- [20] I. M. Tolic-Norrelykke, E.-L. Munteanu, G. Thon, L. Oddershede, and K. Berg-Sorensen, *Phys. Rev. Lett.* **93**, 078102 (2004).
- [21] F. Gittes and F. C. MacKintosh, *Phys. Rev. E* **58**, R1241 (1998).
- [22] B. Fabry, G. N. Maksym, J. P. Butler, D. Navajas, N. A. Taback, E. J. Millet, and J. J. Fredberg, *Phys. Rev. E* **68**, 041914 (2003).
- [23] J. P. Butler *et al.*, *Am. J. Physiol.: Cell Physiol.* **282**, C595 (2002).
- [24] J. T. Finer, R. M. Simmons, and J. A. Spudich, *Nature (London)* **368**, 113 (1994).
- [25] Y. Z. Ma and E. W. Taylor, *Biophys. J.* **66**, 1542 (1994).
- [26] S. M. Mijailovich, J. P. Butler, and J. J. Fredberg, *Biophys. J.* **79**, 2667 (2000).
- [27] The typical mechanical load of a single focal adhesion has been determined in Ref. [28] as 10 nN. We assume here that only one fiber attaches to each focal adhesion. In the simplest model, a stress fiber consists of actin filaments, which are dynamically cross-linked by myosin motor proteins. A single myosin molecule produces an average force of  $\bar{f}_m = f_m \epsilon_m = 1$  pN. We can therefore deduce that about  $N_m = 10^4$  myosins must act in parallel within each stress fiber.
- [28] N. Q. Balaban, U. S. Schwarz, D. Riveline, P. Goichberg, G. Tzur, I. Sabanay, D. Mahalu, S. Safran, A. Bershadsky, L. Addadi, and B. Geiger, *Nat. Cell Biol.* **3**, 466 (2001).
- [29] Micrographs of the cytoskeleton show that stress fibers have a broad distribution of geometric dimensions. The averaged size parameters used in our model are consistent with experiments on single stress fibers, performed by Deguchi *et al.* [16].
- [30] Deguchi *et al.* [16] measured the tensile properties of single stress fibers by *in vitro* manipulation with cantilevers. The presented range of Young moduli describes only the linear part of a nonlinear stress-strain relation found in their experiments. In order to fit our data, we have to assume a significantly smaller value of only 100 kPa for a living fiber. However, this is not unreasonable since the single-fiber stretching experiments were performed under nonphysiological, ATP-deprived conditions. It is known that the myosin cross bridges then adopt a rigor state of high static stiffness [26].
- [31] From Ref. [28], the typical time constant associated with the turnover of focal adhesions has been determined as 200 s. The buildup time for the complete stress fiber must be longer than that for one of its components.
- [32] The number of fibers typically attached to a coated microbead has been estimated from micrographs. See, for example, Fig. 1 in Ref. [5].
- [33] This compares well with data from rheological creep experiments with cytoskeleton-bound microbeads. From Ref. [34] we estimate a value of  $k_w = 1.3$  nN/ $\mu$ m.
- [34] A. R. Bausch, F. Ziemann, A. A. Boulbitch, K. Jacobson, and E. Sackmann, *Biophys. J.* **75**, 2038 (1998).
- [35] In future experiments, direct information about the noise in the stress fiber network might be obtained by observing spatial fluctuations of ECM-bound markers close to focal adhesions (compare Sec. VIII). If in addition to the Young modulus of the purely elastic substrate, the distance between the marker and focal adhesion is known, the amplitude of the force fluctuations can be determined.
- [36] This value agrees well with average drift velocities estimated from our measured bead trajectories.
- [37] S. Denisov, J. Klafter, and M. Urbakh, *Phys. Rev. E* **66**, 046217 (2002).